Talanta 301 (2026) 129346

Contents lists available at ScienceDirect

Talanta

journal homepage: www.elsevier.com/locate/talanta

Analytical quality by design in the development of a paper-based microfluidic device for iron (II) determination as an impurity in iron (III) pharmaceuticals

Muhammad Waqar [a], Benedetta Pasquini [b], Serena Orlandini [b], Lucrezia Floris [a], Sandra Furlanetto [b], Roberto Gotti [a,*]

[a] Department of Pharmacy and Biotechnology, University of Bologna, Via Belmeloro 6, 40126, Bologna, Italy
[b] Department of Chemistry "Ugo Schiff", University of Florence, Via U. Schiff 6, 50019, Sesto Fiorentino, Italy

ARTICLE INFO

Keywords:
Microfluidic paper-based analytical device
Iron (II) impurity
1,10-Phenanthroline
Analytical quality by design
Method Operable design region
Validation

ABSTRACT

A microfluidic paper-based analytical device (μPAD) was developed for the quantitation of ferrous ions (Fe^{2+}) and total iron in iron sucrose administered in iron deficiency anemia. The elemental iron content is 20 mg/mL and USP established a limit of Fe^{2+} as 0.4 % (w/v). The μPAD allowed the quantitation of Fe^{2+} by complexation with 1,10-phenanthroline, forming an orange-red complex analysed by imageJ®. For total iron determination, ferric ion (Fe^{3+}) was reduced to Fe^{2+} using ascorbic acid prior to complexation. The device was prepared on chromatographic paper by using the wax printing method. The dimensions of channels and detection zones as well as reagents/sample volumes were optimized using an Analytical Quality by Design (AQbD) approach, focusing on two critical analytical procedure attributes: mean intensity of the colour developed in the detection zones and homogeneity of the colour. By implementing the AQbD, the Method Operable Design Region was defined to account for model uncertainty and experimental variability. The optimized method was linear over 0.10–0.50 mM for Fe^{2+} and 2.0–8.0 mM for total iron, with limits of quantitation of 0.10 and 1.60 mM, respectively. Method performance was evaluated for selectivity, range, sensitivity, trueness, and robustness. Application to commercially available iron sucrose injections showed the accurate quantitation of Fe^{2+} impurities, with results statistically comparable to a validated capillary electrophoresis method. The developed μPAD is a low-cost, portable, and reliable platform for iron determination in pharmaceutical samples, suited to resource-limited settings.

1. Introduction

Paper is an excellent substrate for microfluidic chips since the flow of fluid is governed by capillary action rendering the need of external pumps obsolete; in addition, due to the high surface to volume ratio, paper can store reagents and acts as a natural filter for samples [1–4]. Several techniques have been made available for the manufacturing of the chips allowing to easily prepare the paper-based microfluidic devices (μPADs); the wax printing is considered as one of the most convenient as it uses a non-toxic wax ink in a commercially available printer to define on the paper the hydrophobic pattern of the channels of the device [1,2,5]. The paper must be heated on a hot plate or in an oven to allow the wax ink to penetrate the entire thickness of substrate thus ensuring the complete hydrophobization [6]. The disposal of used μPADs is simple and their straightforward incineration, even when used for infectious samples, make them suitable for applications in medical and environmental diagnostics, food safety and therapeutic drug monitoring [2,7,8].

The most common detection techniques are electrochemical, fluorescence and colorimetric sensing [9,10]. In electrochemical sensing, the sample is driven by capillary action to the working electrode where the signal is obtained [11–13]. The approach allows for high sensitivity, fast response, and opportunity for multiplexed analysis [14], however it requires trained personnel and the use of a portable potentiostat which is one of the drawbacks in μPADs applications at the point-of-need (PON). Similarly, fluorescence detection, although has high sensitivity, suffers from the background noise from the paper substrate and high cost of fluorescent markers [15]; in addition, it requires for a suitable detector

* Corresponding author.
E-mail address: roberto.gotti@unibo.it (R. Gotti).

https://doi.org/10.1016/j.talanta.2025.129346
Received 18 October 2025; Received in revised form 19 December 2025; Accepted 30 December 2025
Available online 4 January 2026

for the fluorescence readout [16]. By far, colorimetric sensing is the most common detection technique used for paper devices providing high-contrast and bright readings. This approach involves colour change following a reaction which can be detected by eye (yes/no answer) or accurately quantified by using a suitable instrument as a digital scanner or more conveniently at PON hand-held devices or smartphone camera [17–19]. To ensure a μPAD performs reliably for the intended analytical purpose, its architecture must be optimized encompassing parameters like channels and detection zones dimensions. Several studies have been made available concerning design configurations and reagent layouts of μPADs. Carrio et al., [20] studied the spreading of wax in the paper before and after heating according to the temperature and established a correlation among them. Similarly, the wicking speed of the fluid has been studied by proposing incorporation of grooves as obstacles or by varying the width and length of the hydrophobic barriers [21,22]. Conventionally the optimization of μPADs parameters have relied on the one-variable-at-a-time approach [21]; this methodology presents significant limitations since changing a single parameter while holding the others constant, does not capture for their possible interactions thus neglecting their synergistic influence on the final analytical results. Only very recently the fabrication of a μPAD has been reported by a machine learning-based cyclic optimization strategy [23]. Design of experiments (DoE) is nowadays a well-known procedure that evaluates possible interactions among variables [24]; by linking variables to responses, DoE allows an in-depth understanding of the system under investigation. While DoE enables the experiments planning and the system description using response surfaces, Analytical Quality by Design (AQbD) is an ideal framework for the optimization of a complex analytical procedure as it focuses on the development of methods ensuring controlled and high-quality analytical results [25]. The application of the principles of AQbD enables the integration of advanced risk management tools, ensuring reliable and robust analytical results that are essential for supporting critical decision-making throughout the product lifecycle. In the present study, the AQbD has been applied to optimize the device architecture and reagent parameters for the development of a μPAD addressed to the quantitation of Fe^{2+} as an impurity in iron sucrose nanoparticles (20 mg/mL of elemental iron), a drug used in patients with chronic kidney disease [26]. According to United States Pharmacopoeia (USP), the content of Fe^{2+} in the iron sucrose preparation should not exceed 0.4 % (w/v) [27]. The USP official method is based on polarography whose application raise environmental and health concerns, thus the development of alternative methods based on more sustainable techniques is highly desirable. The quantitation of iron including the Fe^{2+}/Fe^{3+} speciation by μPADs has been reported in various samples as natural waters [28], serum [29] and urine samples [30] as well as in wine since the Fe^{3+}/Fe^{2+} ratio is a marker of the rate at which the contained polyphenols can remove oxygen during the wine-making process [31]. The colorimetric detection of Fe^{2+} in the μPAD has been reported by means of the complexation using 1,10-phenanthroline (Phe) or bathophenanthroline [31,32], and ferrozine [29], whereas Fe^{3+} has been determined by complexation by the original reagent naphthalene-3-hydroxy-4-pyridione [28] or after reduction to Fe^{2+} by hydroxylamine and subsequent complexation with the above reported complexing agents [29,31,32]. In the present study Phe was used as the complexing agent for the direct quantitation of the drug impurity Fe^{2+} in the pharmaceutical samples; to establish the quantity of total iron, Fe^{3+} was reduced to Fe^{2+} using ascorbic acid before complexation with Phe. The colour intensity in the reaction zone of the μPADs was determined using mean grayscale analysis in ImageJ® software after scanning the device. The method was cross validated by determination of Fe^{3+} and Fe^{2+} in the drug preparation by a capillary electrophoresis method [33].

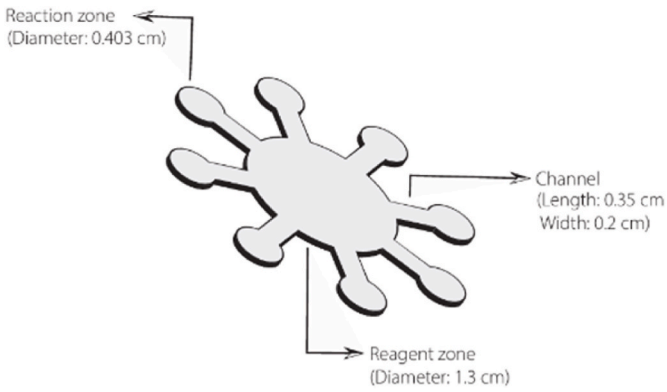

Fig. 1. Scheme and dimensions of the optimized μPAD.

2. Experimental

2.1. Reagents and materials

1,10-Phenanthroline (≥99 %), ascorbic acid (≥99 %), iron(III) chloride hexahydrate (≥99 %), iron(II) sulfate heptahydrate (≥99 %), cadmium carbonate (98 %), cobalt(II) chloride hexahydrate (≥99 %), chromium(III) chloride hexahydrate (≥98 %), nickel(II) chloride hexahydrate (≥98 %), zinc chloride (≥98 %), phosphoric acid (≥85 %), sodium tetraborate decahydrate, sodium hydroxide, 1,2-diaminocyclohexanetetra-acetic acid monohydrate (CDTA), suprofen and acetic acid were all purchased from Sigma-Aldrich (Milan, Italy) and used without any further purification. Deionized water was obtained with a Milli-Q system (Millipore, Milford, MA, USA). Acetate buffer (2.0 M) pH 4.8 was prepared by using sodium acetate trihydrate and acetic acid. Phe (50 mM) and ascorbic acid (0.50 M) solutions were freshly prepared in acetate buffer every day. The stock solutions of Fe^{2+} (10 mM) and Fe^{3+} (50 mM) were freshly prepared every day in 0.10 M phosphoric acid and diluted in the same solvent to obtain standard solutions for calibration curves and for recovery experiments. Similarly, standard solutions of Cd^{2+}, Co^{2+}, Cr^{3+}, Ni^{2+} and Zn^{2+}, were prepared in 0.10 M phosphoric acid and properly diluted to be spiked to iron solutions, for selectivity experiments.

Whatman™ chromatography paper (CHR 1) by Sigma-Aldrich was used as the substrate for printing the μPAD devices using the Xerox ColorQube 8570 wax printer (this model is discontinued; however refurbished sets and wax ink can be obtained from the manufacturers). The paper devices were baked in a laboratory oven at 145 °C for 3.5 min before the use. Designs of the devices were prepared using Adobe Illustrator software version 29.8.1 (Adobe Systems Inc., San Jose, CA, USA). Images of the devices for the response acquisition were obtained by a Canon LiDE scanner 400 (Canon Inc., Tokyo, Japan), and the image analysis was performed using ImageJ® version 1.54g (National Institutes of Health, Bethesda, USA).

2.2. Analytical procedure

Phenanthroline solution (50 mM) was drop-cast (25 μL) onto the central reagent zone (Fig. 1) of the μPAD and allowed to dry for 20 min at room temperature. Ascorbic acid solution (0.50 M) was then drop-cast (1.15 μL) onto the designated reaction zones and dried at room temperature for 10 min. For analysis, either standard solutions of Fe^{2+} or Fe^{3+} or drug sample solutions, were drop-cast (0.75 μL) onto the reaction zones and allowed to dry for 10 min. Upon reaction, the characteristic red-orange complex was formed. The devices were scanned by Canon LiDE 400 scanner, and the images were analysed in ImageJ®. In ImageJ® software, a 30 × 30-pixel circular region of interest (ROI) (for optimized devices) was directly superimposed over each reaction zone, and the mean grayscale intensity was recorded using the Analyze and

Variables category	<	Units	Homogeneity	Absolute mean Intensity	St. dev. of Intensity	Sensitivity	Easy	Fast	Knowledge	Criticality	Total score
Sample/Reagents	Reagent (Phe) volume	uL	2	2	1	2	3	2	2	pCPP	14
	Sample volume	uL	2	3	2	3	2	2	2	pCPP	16
	Reducing agent volume	uL	2	2	1	2	3	2	2	pCPP	14
Dimensions of device	Reagent zone (central) diameter	cm	1	1	1	1	2	1	2	PP	9
	Reaction zone diameter	cm	3	3	2	3	2	2	2	pCPP	17
	Channel length	cm	2	2	1	1	3	1	2	pCPP	12
	Channel width	cm	2	2	1	1	2	1	2	pCPP	11
Device manufacturing	Baking temperature	°C	1	1	1	1	2	1	1	PP	8
	Baking time	min.	1	1	1	1	2	1	1	PP	8

Fig. 2. Cause-effect matrix.

Measure tool. The Mean Intensity of the colour (hereafter referred as Mean Intensity) was given as the average pixel intensity within the selected ROI. The homogeneity of the colour (hereafter referred as Homogeneity) was given by ImageJ® as the standard deviation (SD) of pixel intensities within the ROI.

2.3. Preparation of the drug samples

The drug product belongs to the class of parenteral non-biological complex drugs administered in the treatment of iron deficiency anaemia. The pharmaceutical is a brown, sterile, aqueous complex of polynuclear Fe^{3+}-hydroxide in sucrose [34], that must be treated before the analysis to completely release iron from the nanoparticles; thus an aliquot of 100 µL was transferred into 10 mL volumetric flasks, followed by the addition of 68.5 µL phosphoric acid (85 %). The mixture was vortexed for 2 min until a clear yellow solution was obtained. The solution was diluted to volume (10 mL) with deionized water and directly applied to the reaction zones of the µPAD for analysis. For recovery experiments, Fe^{2+} and Fe^{3+} standard solutions were added into the prepared drug solutions and then analysed on the µPAD. The standard solutions of iron (Fe^{2+} and Fe^{3+}) were prepared using freshly acquired certified reference compounds.

2.4. Capillary electrophoresis

Capillary electrophoresis was applied to the same samples analysed by µPAD for comparison. The method was developed and validated as described in a previous paper [33]. Electrophoretic experiments were performed by the CE7100 instrument from Agilent Technologies (Waldbronn, Germany). The data were collected on a personal computer, equipped with the OpenLab software by Agilent Technologies. Fused-silica capillaries (50 µm id, 64.5 cm total length, 56 cm length to the detector) were from CM Scientific (Silsden, UK). The separations were performed at a constant voltage of 25 kV and the cartridge temperature was at 25 °C. The detection was carried out by using the on-line DAD detector and the quantitation was performed at the wavelength of 265 nm (bw 10 nm). Hydrodynamic injections were performed at 50 mbar for 10 s. New capillaries were conditioned by flushing sequentially 1 M sodium hydroxide, 0.1 M sodium hydroxide and deionized water in the order, for 10 min each. Between the injections the capillary was rinsed with 0.1 M sodium hydroxide (2 min), deionized water and running buffer for 3 min each. The running buffer was an aqueous solution of 60 mM sodium tetraborate (pH 9.3). The separations were performed once the samples were subjected to the complexation in the presence of an internal standard (suprofen at the final concentration of 2 µg/mL).

2.5. Statistical analysis and software

NemrodW software (NemrodW, LPRAI sarl, Marseille, France) was used for the DoE and the statistical analysis in the screening phase and in the robustness study, while MODDE Pro Version 13.1 software (Sartorius Data Analytics, Göttingen, Germany) was used in the optimization phase and for the identification of Method Operable Design Region (MODR) by means of Monte Carlo simulation.

3. Results and discussion

3.1. Optimization of the iron analysis

The present study was addressed to develop under the AQbD framework a µPAD for the quantitation of total iron (Fe^{2+} plus Fe^{3+}) and Fe^{2+} in iron sucrose pharmaceutical samples using colorimetric detection. Since Fe^{2+} is considered as the pharmaceutical impurity, the quantitation must be performed at the impurity level established by USP [27]. 1,10 - Phenanthroline was selected for the Fe^{2+} detection and quantitation as it is one of the best complexing agents for its colorimetric determination as due to the high complex stability and detectability in the visible region of the spectrum. The complexation of Fe^{2+} with Phe results in the formation of stable orange-red coloured complex [35] which is easily distinguishable onto the paper substrate. The quantitation of Fe^{3+} can be conveniently based on its reduction to Fe^{2+} to establish the total iron amount in the sample. The reduction can be carried out using different agents; among them ascorbic acid and hydroxylamine are the most applied, however the latter was not considered in the present study because of its toxicity [36]. By a preliminary evaluation, Phe was prepared in acetate buffer (pH 4.8) as the obtained complex resulted to be stable within a working day in the dark [37,38]. The µPAD was fabricated using chromatographic paper CHR No. 1 by means of a wax printer. In Fig. 1 is reported the scheme of the optimized device: the number of the reaction zones was established as the best compromise between the maximum availability of determinations for a single device and its physical dimension. Aliquots of Phe solution were drop casted into the reagent central zone (Fig. 1); then ascorbic acid and the sample solutions containing both iron species, were introduced in the reaction zones where detection takes place, after complexation. The colour developed in the reaction zones was scanned and the collected images were treated by ImageJ® for acquisition of the Mean Intensity as the response directly related to the concentration of total iron. The selective determination of Fe^{2+}, was obtained by applying the same procedure avoiding dropping cast the ascorbic acid solution. Introducing as first event the reagent Phe in the central zone of the device was found to be beneficial in obtaining uniformity of the colour developed in the peripheral reaction zones avoiding the so-called coffee-ring effect [39]. The samples were directly drop casted into the reaction zones to achieve

higher sensitivity with respect to the introduction into the central zone of the device.

3.2. AQbD-assisted optimization of the μPAD design

In the experiments for iron determination, the variables *i.e.,* sample/reagent volumes as well as the dimensions of the device, affect the Mean Intensity and its precision. An AQbD approach was used to manage the risk associated to the change in the variables values and to obtain a reliable device using DoE methodology to plan the experiments. According to the ICH Q14 guideline [25], the Analytical Target Profile (ATP) was established to ensure robust and accurate quantitation of Fe^{2+} and total iron, setting linearity ranges of 0.10–1.0 mM and 2.0–10.0 mM, and limits of quantitation below 0.10 and 2.0 mM for the two analytes, respectively.

3.2.1. Risk assessment

The risk assessment step involves defining the critical procedure attributes that are essential for the device performance, as well as identifying the experimental parameters that significantly impact the device analytical performance and could pose a hazard to the ATP. The risk analysis step allows the identification of the potential Critical Procedure Parameters (pCPPs) to be selected among all possible procedure parameters by means of simple risk analysis tools [40]. In this research the cause-effect matrix (Fig. 2) was used. The probability that a given parameter may cause harm can be assessed either quantitatively or qualitatively. The red color in the reported matrix is typically associated with a high probability of occurrence. As is shown in Fig. 2, the variables were grouped into three functional categories indicating their role in the μPAD: Volume of sample/reagents; Dimensions of the device; Device manufacturing conditions. Within the sample/reagents category, the volumes of chromogenic reagent (Phe), reducing agent (ascorbic acid) and iron containing sample, were considered. These factors affect the local flow of the reagents in the channels of the μPAD, and thus impacting colour development and uniformity once the complexation of Fe^{2+} has occurred. In device dimensions category, reagent zone diameter, reaction zone diameter, channel length and channel width were evaluated. These factors influence fluid flow and reagent diffusion and ultimately have an impact on homogeneity and uniformity of the colour developed. Baking time and temperature were considered as parameters under device manufacturing since they affect wax penetration and hydrophobic barrier integrity which can impact fluid migration and reagent retention.

Nine parameters were scored against multiple performance criteria. Sensitivity, ease of implementation and speed were also scored according to the practical feasibility of using the device under routine conditions. Scores were based on brainstorming and operational knowledge gathered during preliminary investigations. Each performance criteria were subjectively scored on a scale from 1 to 3 (where 1 indicates a low impact, 2 a medium impact, and 3 a high impact); as for knowledge criterion, the scores were assigned inversely (1, 2 and 3 indicating high, medium, and low, respectively). A total criticality score was then calculated by summation of all scores for each parameter and for knowledge. It was assumed that factors which potentially do not affect the responses consistently scored below 10 and hence this was selected as a cut-off value. The parameters which scored above 10 were classified as pCPPs and parameters scoring below this threshold were classified as Procedure Parameters (PPs) and were not prioritized for optimization. Matrix analysis highlighted six pCPPs namely, Reagent (Phe) volume; Sample volume; Reducing agent (ascorbic acid) volume; Channel length; Channel width; and Reaction zone diameter which could influence method responses and hence merit deeper study. Baking time, baking temperature and reagent zone diameter scored low in cause-effect matrix and hence were considered as non-critical under current conditions. This critical assessment helped focus on the pCPPs reducing experimental complexity.

Table 1
Experimental domain during the risk evaluation step.

Parameter	Abbreviation	Units	Type	Settings
Reagent (Phe) volume	Rea_v	μL	Quantitative	21 to 25
Sample (drug) volume	Sam_v	μL	Quantitative	0.30 to 0.50
Reducing agent volume	Red_v	μL	Quantitative	0.80 to 1.0
Reaction zone diameter	Rea_d	cm	Quantitative	0.45 to 0.50
Channel length	Cha_l	cm	Quantitative	0.30 to 0.40
Channel width	Cha_w	cm	Quantitative	0.20 to 0.25

To evaluate and optimize the analytical performance of the μPAD for iron quantification, three potential critical Analytical Procedure Attribute (cAPA) were considered: (i) Mean Intensity; (ii) Homogeneity; and (iii) Standard deviation (SD) of the Mean Intensity. While iron determination served as a target application in this study, the selected responses have a broader relevance to the colorimetric detection in μPAD being intrinsically linked to the device reliability.

(i) The Mean Intensity (mean grayscale intensity) is the total signal generated by the colorimetric complexation and serves as a direct surrogate of sensitivity and detectability. A stronger colour signal (hence lower Mean Intensity value) increases confidence in measurements especially at lower concentrations.
(ii) Homogeneity is related to the uniform distribution of the colour inside the reaction zone which is crucial to minimize spatial bias during image capture and analysis by ImageJ®. The Homogeneity was extracted by considering a circular window of 30 x 30 pixels (optimized conditions) and was defined as standard deviation of pixel intensity within that window. Non-uniform colour distribution can skew the pixel-based reading in ImageJ®, thereby introducing variability unrelated to analyte concentration and hence decreasing the accuracy of measurements.
(iii) The SD of Mean Intensity was chosen as a response to assess the variability in colorimetric signal observed in replicate reaction zones subjected to the same experimental conditions. This response was intended to capture how consistently the same experimental parameters yielded the same signal outputs. The underlying objective was to determine whether this response could be attributed to controllable design or condition parameters, which ultimately could be optimized by AQbD.

The risk evaluation to identify the pCPPs was carried out by means of a DoE. A first order polynomial model including the principal effects of the pCPPs: Reagent Volume (x_1); Sample Volume (x_2); Reducing Agent Volume (x_3); Reaction Zone Diameter (x_4); Channel Length (x_5); Channel Width (x_6) and the interaction effects between Sample Volume and Reaction Zone Diameter (x_2 x_4); Reducing Agent Volume and Reaction Zone Diameter (x_3 x_4); Reaction Zone Diameter and Channel Length (x_4 x_5); Channel Length and Channel Width (x_4 x_6) (equation (1)) was hypothesized.

$$Y = b_0 + b_1{*}x_1 + b_2{*}x_2 + b_3{*}x_3 + b_4{*}x_4 + b_5{*}x_5 + b_6{*}x_6 + b_{24}{*}(x_2{*}x_4) + b_{34}{*}(x_3{*}x_4) + b_{45}{*}(x_4{*}x_5) + b_{56}{*}(x_5{*}x_6) \quad \text{(Eq. 1)}$$

The experimental domain explored is reported in Table 1. A 21-run D optimal experimental matrix derived from a Full Factorial Design (FFD) was used to estimate the coefficients of the model and Table S1 (Supplementary Data) reports the experimental plan and the obtained responses. The analysis of variance (data not shown) indicated that the model was significant only for the response Mean Intensity. Fig. 3 shows the graphical analysis of the effects and provides information on the significant variations of the factors: bars that extend beyond the two vertical lines, representing the variation in response due to experimental error, correspond to the effects that were found statistically significant.

As for Mean Intensity the effects were significant for the pCPPs Sample Volume and Reaction Zone Diameter, whereas interaction

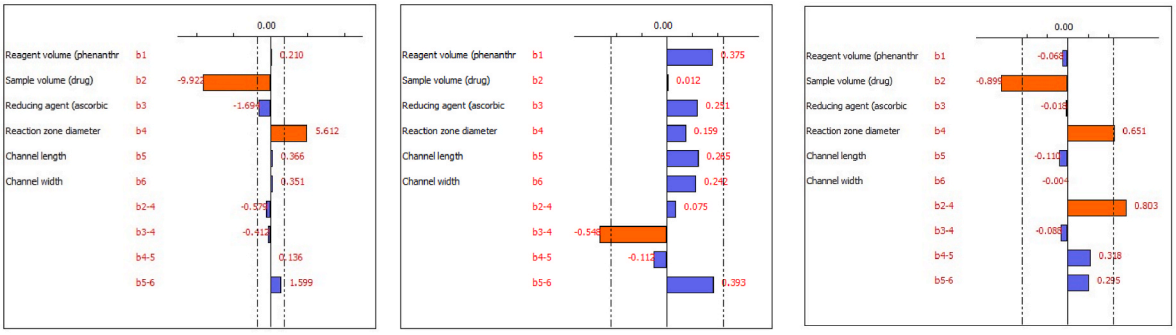

Fig. 3. Graphic analysis of effects for response (left) Mean Intensity, (central) SD of Mean Intensity (St.dev.) and (right) Homogeneity (Homo).

Table 2
Experimental domain during the optimization step.

Parameter	Abbreviation	Units	Type	Settings
Reagent (Phe) volume	Rea_v	µL	Constant	25
Sample (drug) volume	Sam_v	µL	Quantitative	0.50 to 0.90
Reducing agent volume	Red_v	µL	Quantitative	1.0 to 1.2
Reaction zone diameter	Rea_d	cm	Quantitative	0.40 to 0.46
Channel length	Cha_l	cm	Constant	0.35
Channel width	Cha_w	cm	Constant	0.20

effects were not statistically significant. To minimize the response and approach the ATP, Sample Volume should be moved to the high level while the Reaction Zone Diameter towards the low level.

Regarding SD of Mean Intensity, the sole significant effect was the negative interaction between Reducing Agent Volume and Reaction Zone Diameter. As it concerns Homogeneity, a negative effect was displayed for Sample Volume, contrasting with the positive correlation observed for Reaction Zone Diameter; a significant interaction between these two parameters was detected. To minimize the SD of Mean Intensity, the Reaction Zone Diameter and Reducing Agent Volume had to be set at the low values, whereas to minimize the value of Homogeneity, the Sample Volume had to be set at the high level while that of the Reaction Zone Diameter towards low level.

According to the obtained information the Critical Procedure Parameters (CPPs) were found to be Sample Volume, Reducing Agent Volume and Reaction Zone Diameter. These CPPs were selected to carry out the risk reduction by means of the response surface methodology (RSM) using a Central Composite Design (CCD). The experimental domain explored for the optimization step is reported in Table 2, while in Table S2 is reported the experimental plan with the obtained responses. In this case a second-degree polynomial model was hypothesized, and it is reported in Equation (2).

$$Y = b_0 + b_1{*}x_1 + b_2{*}x_2 + b_3{*}x_3 + b_{11}{*}(x_1{*}x_1) + b_{22}{*}(x_2{*}x_2) + b_{33}{*}(x_3{*}x_3) + b_{12}{*}(x_1{*}x_2) + b_{13}{*}(x_1{*}x_3) + b_{23}{*}(x_2{*}x_3) \quad \text{(Eq. 2)}$$

The models were significant for Mean Intensity and Homogeneity (the graphic representations are reported in Fig. S1) whereas for SD of Mean Intensity a weaker model was obtained, and the response was not considered in the further investigation.

As shown in Fig. S1 the Mean Intensity response is minimized with high levels of the parameter Sample Volume and by decreasing the levels of the Reaction Zone Diameter. All the investigated values of the Reducing Agent Volume were found to be suitable for approaching the ATP. For Homogeneity, minimization requires high values of Sample Volume and low values of the Reaction Zone Diameter.

To define the Risk Acceptance and thus the Method Operable Design Region (MODR), the Monte Carlo simulation, implemented in the MODDE Pro software, was used. This computational algorithm allows to estimate the possible outcomes of an uncertain event. The Monte Carlo Risk Analysis which started from the models obtained by RSM, considers the uncertainty in factors setting, the estimated uncertainty for the model parameters and propagates the prediction error from parameters to responses. Monte Carlo simulation allowed the probability map to be drawn according to a selected risk of failure.

Fig. 4 shows the probability map for the responses Mean Intensity and Homogeneity calculated for a 5 % risk of failure. The green colour identifies the region where all response objectives are met (the MODR); the dotted line defines the biggest regular MODR, a simpler space to be experimentally managed. The cross identifies the most robust experimental conditions whereas, the double concentric circle identifies the best performing experimental conditions *i.e.*, the variables setting which correspond to response values closest to the target.

For the MODR, the desirability plot is also reported in Fig. S2 (Supplementary Data); it shows how the objective targets of the two

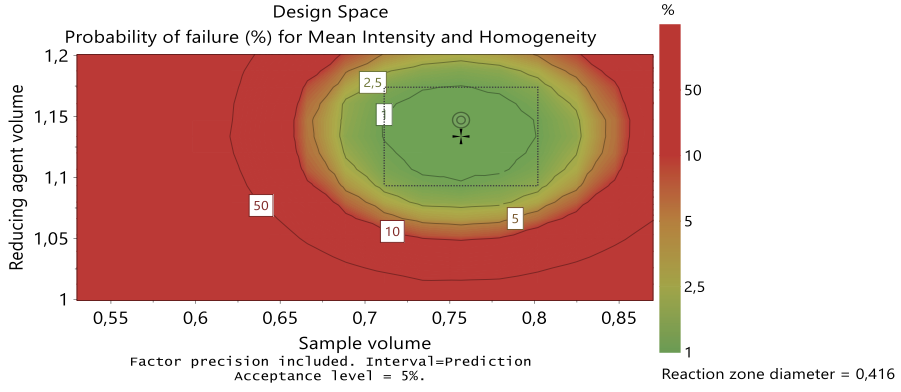

Fig. 4. Probability plot for the responses Mean Intensity and Homogeneity. The cross identifies the robust conditions; the circle identifies the optimum experimental conditions. The validation was carried out at the optimum conditions and at the conditions corresponding to the rectangle edges.

Table 3
Conditions at the four edges of MODR and optimum conditions*.

Exp No	Sample volume[1]	Reducing agent volume[1]	Reaction zone diameter[2]
1	0.71	1.09	0.424
2	0.80	1.09	0.400
3	0.71	1.19	0.400
4	0.80	1.19	0.424
5*	0.75	1.15	0.404

[1] μL.
[2] cm.

responses are fulfilled within the MODR. In the plot, "1" equals all objectives fulfilled whereas "0" equals no objectives fulfilled thus, the higher the value, the closer are all the responses to their target value. Since the plot only includes regions with desirability values equal or higher than 0.95, then MODR domain includes solutions that are both robust and very close to the targets.

Robustness was assessed around the optimum conditions by means of a Plackett Burman design for 3 factors. The factors variation range was set according to the regular MODR. Each experiment was replicated to have an estimation of the experimental variance. The experimental plan together with the obtained responses values are reported in Table S3 (Supplementary Data) and ANOVA (Table S4–S6). The data show that all the models are not statistically significant thus indicating the μPAD method robustness.

3.3. Method validation

To validate the MODR, the analytical performance of the μPAD was tested at the optimized conditions *i.e.,* reagent zone diameter at 1.30 cm; reaction zones diameter at 0.404 cm; channels length at 0.35 cm; channels width at 0.20 cm; reagent volume 25 μL; sample volume at 0.75 μL; reducing agent volume at 1.15 μL. In addition, the validation was also carried out at the conditions corresponding to the edges of the regular MODR (Table 3). According to the ICH Q2(R2) [41], the parameters evaluated were selectivity, range, detection limit (DL), quantitation limit (QL), trueness, and precision (robustness was also assessed). For each of the considered parameters, the Mean Intensity value was assumed as the mean of four independent reaction zone readings (n = 4). Below are discussed and reported the results of the performance parameters evaluated under optimum conditions. As for the other tested conditions the results (data not shown) agreed with those at the optimum one demonstrating that inside the MODR all conditions fulfil the ATP requirements.

3.3.1. Selectivity, range, detection, and quantitation limits

The method selectivity is inherently supported by the specific complexation of Fe^{2+} with Phe [33,35]; however, to investigate the potential interferences from other cations known to complex with Phe, a selectivity study was undertaken. Standard Fe^{2+} solutions (0.3 mM, the assay concentration) were individually spiked with Cd^{2+}, Co^{2+}, Cr^{3+}, Ni^{2+}, and Zn^{2+} each at the concentration of 0.015 mM (5 % relative to the analyte). The concentration of Fe^{2+} determined by μPAD method in these spiked mixtures did not differ significantly from those in the unspiked standards confirming the selectivity of the method. These results are summarized in Table S7 and Fig. S3 (Supplementary Data). A further demonstration of selectivity is provided by the recovery studies and comparison of the results on real samples analysis with those from an orthogonal CE method as described and discussed in the due section (3.4. *Analysis of real samples*) [41]. The range of the μPAD procedure *i.e.,* the interval between the lowest and the highest results in which the method provides a suitable level of trueness and precision, was evaluated for Fe^{2+} and total iron within 0.10–0.50 mM and 2.0–8.0 mM, respectively. Based on the regression analysis the QLs and the DLs were assessed as 10σ/S, and 3.3σ/S respectively. The meaning of σ is the standard deviation of the response and S is the slope of the dosing range [25]. The data obtained in the optimum conditions are reported in Table 4. These values are in the same order of previous studies involving architectures with horizontal fluid flow as in our μPAD. Dortez et al., reported a DL of 3 μg/mL (0.05 mM) in the determination of Fe^{3+} following reduction to Fe^{2+} by hydroxylamine and complexation with ferrozine. To enable application to human serum they introduced an immunomagnetic beads preconcentration step which improved sensitivity by one order of magnitude [29]. In an application of μPAD for the analysis of heavy metals in water, Fe^{3+} was detected at the DL of approximately 0.01 mM using bathophenanthroline as the complexing agent [42]. Ogawa et al., reported the QL of 0.7 mM in the determination of iron in hot water spring [43], and Wendimu et al., found a DL of 0.08 mM in welding fumes [38]. Using these simple device fabrication techniques and architecture, simultaneous determination of multiple samples is possible. Conversely, some studies have focussed on developing test spot-type μPAD systems where sample and reagent diffusion is limited. For instance, by developing a test-spot type μPAD whose hydrophobic barrier was created using photolithography, Asano and Shiraishi reported a DL of about 4 μM for Fe^{2+} assay using Phe relying on high sample volumes (20 μL) [44]. Similar diffusion control, facilitated by lamination-based test-spot design was employed by Mesquita et al., for analysis of iron in water, urine, and wine, achieving DLs in the μM range [28,30,31]. The similar test-spot architecture, implemented by cetyltrimethylammonium bromide-modified silver nanoparticles on the paper substrate, allowed Fe^{3+} determination in environmental and biological samples with DL in the sub-μM range [32]. A comparison of the achieved figures of merit of the present μPAD procedure with those from the previous similar studies is reported in Table S8 (Supplementary Data).

Table 4
Linear range[1], linear regression equations, detection and quantitation limits.

	Range	Equation	r^2	DL	QL
Iron (II)	0.10–0.50	$y^{(2)} = (-58.14 \pm 1.80)x^{(3)} + (249.29 \pm 0.61)$	0.997	0.03	0.10
Total Iron	2.00–8.00	$y = (-6.26 \pm 0.22)x + (202.55 \pm 1.22)$	0.996	0.50	1.60

[1] mM.
[2] y is mean grayscale intensity (arbitrary unit).
[3] x is the concentration.

3.3.2. Trueness and precision

Trueness and precision were evaluated for Fe^{2+} at the concentration of 0.10, 0.30 and 0.50 mM and for total iron at 2.0, 5.0 and 8.0 mM; each of the three levels was replicated by preparing three independent solutions (n = 3) and applying optimum conditions. The obtained data are reported in Table S9 (Supplementary Data). For Fe^{2+} determination the trueness was within the range of 93.3–105.4 %. Precision was confirmed by low RSD values, ranging within 2.34–6.0 %. The highest variability was observed at the lowest tested concentration which is expected due to proximity to the limit of detection. Similarly, the method trueness in analysis of total iron was within 89.6–104.4 % (RSD values 0.50–2.51 %). These figures of merit are comparable to those reported in previous μPAD studies [29,43,44].

3.4. Analysis of real samples

The developed method was applied to the determination of Fe^{2+} as an impurity in a pharmaceutical formulation based on iron sucrose nanoparticles (20 mg of elemental iron per mL) [34]. The real sample analysis requires the drug to be treated to release the iron species (Fe^{2+} and Fe^{3+}) while avoiding Fe^{2+}/Fe^{3+} interconversion. In a previous study [33], concentrated hydrochloric acid was used for mineralization of the sample, however it was found that under certain conditions a partial

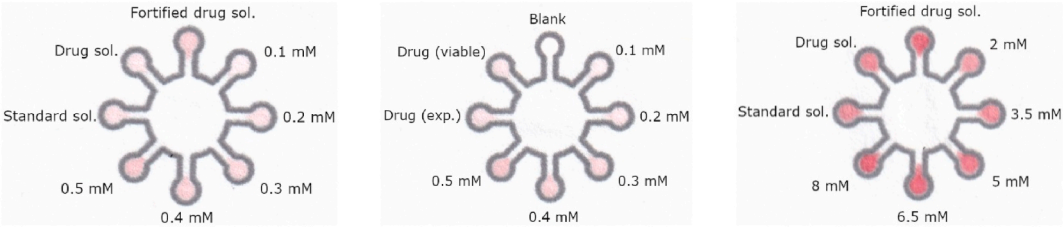

Fig. 5. Typical results of the μPAD analysis of Fe^{2+} and total iron including calibration solutions and sample.

reduction of Fe^{3+} to Fe^{2+} occurred thus the selection of the hydrochloric acid concentration had to be accurately optimized to avoid artifact Fe^{2+} impurity to be produced. Interestingly, according to Merli et al., [45] in the present application it was found that using phosphoric acid instead of hydrochloric acid, the release of iron from the real samples occurred rapidly providing stable solutions and overcoming the interconversion between the iron species. A comparison of the efficiency in releasing iron from the pharmaceutical using hydrochloric and phosphoric acid was carried out. According to our previous study, the real pharmaceutical injections were directly subjected to mineralization using HCl (6 M) under ultrasonication for about 10 min. The solution was properly diluted with water to fit the iron content within the calibration range (the final concentration of HCl in the sample solution was 0.1 M). The obtained sample solutions were analysed for both Fe^{2+} and total iron content, by the proposed μPAD and the results were compared with those from the real samples prepared according to the method optimized in the present study using phosphoric acid for iron release. In Table S10 (Supplementary Data) are reported the results obtained using the two different sample preparation methods indicating no significant difference in the content of Fe^{2+} and total iron.

A typical experimental procedure involves the use of five reaction zones (Fig. 5) for calibration and three for sample analysis. The method was applied to commercially available pharmaceutical products, and in addition an expired sample was analysed. The level of Fe^{2+} in the viable drug preparation was 0.125 mM (RSD = 1.00 %, n = 3) while the total iron was found to be 3.66 mM (RSD = 0.50 %, n = 3). The impurity level was corresponding to 0.035 % (w/v) with respect to the elemental iron in the drug formulation, thus in compliance with the maximum level established by USP as 0.4 % (w/v). In the expired formulation, the content of Fe^{2+} was found to be 0.331 mM (RSD = 3.92 %, n = 3) and the total iron was 3.61 mM (RSD = 5.20 %, n = 3); thus, also the expired sample was found to contain the impurity within the permitted level.

Recovery experiments were carried out on the expired samples by spiking both Fe^{2+} and Fe^{3+} at the levels of 0.20 mM and 3.00 mM, respectively. The recovery was calculated for Fe^{2+} as 90.90 % (RSD = 2.30 %, n = 3) and for total iron as 98.60 % (RSD = 3.90 %, n = 3) suggesting the general reliability of the method. The analytical performance of the μPAD method, were compared with that of an independent approach based on a validated CE procedure [33]. The latter method allows to simultaneously quantify Fe^{2+} and Fe^{3+} upon their complexation with Phe and 1,2-diaminocyclohexanetetraacetic acid, respectively. The two complexes were separated in conventional capillary zone electrophoresis conditions using a borax buffer as a background electrolyte. This method demonstrated in the previous study to be a useful alternative to the official USP method based on differential pulsed polarography, thus was assumed as a reference in the present investigation. The drug preparations and the expired samples were analysed by using CE and the results are shown in Table S11 (Supplementary Data), including a representative electropherogram of an expired drug sample (Fig. S4, Supplementary Data). The results obtained by μPAD were found to be not significantly different (*t*-test) from those by CE suggesting that the application by μPAD is suitable to quantify Fe^{2+} at the impurity level in iron sucrose.

4. Conclusion

The Analytical Quality by Design approach was applied to optimize the architecture and the analytical conditions for the development of a simple and reliable microfluidic paper-based device for quantitation of Fe^{2+} using colorimetric detection thanks to the complexation by phenanthroline; Fe^{3+} was determined after reduction on-paper with ascorbic acid. The method was fully validated showing analytical figures of merit making the system potentially useful for a point-of-need assessment. As reported by the manufacturer the iron sucrose injections, when transferred from the vial and stored in a plastic syringe (either diluted with 0.9 % NaCl or undiluted), are chemically stable for 7 days at controlled room temperature (25 °C ± 2; 4 °C ± 2). The proposed μPAD provides a rapid, instrument-free critical quality check to monitor iron oxidation status, safely enabling the utilization of this 7-day stability data and thus could significantly reduce hospital pharmacy waste of this costly specialty product. This method encompasses the requirements by ICH Q14 and represents a compelling advancement toward decentralized quality control, demonstrating the practical power of microfluidic devices in addressing critical challenges in pharmaceutical quality assurance.

CRediT authorship contribution statement

Muhammad Waqar: Writing – original draft, Validation, Investigation, Formal analysis, Data curation. **Benedetta Pasquini:** Writing – original draft, Investigation, Data curation. **Serena Orlandini:** Writing – review & editing, Investigation, Data curation. **Lucrezia Floris:** Validation, Data curation. **Sandra Furlanetto:** Writing – review & editing, Supervision, Investigation, Conceptualization. **Roberto Gotti:** Writing – review & editing, Writing – original draft, Supervision, Funding acquisition, Data curation, Conceptualization.

Declaration of competing interest

The authors declare that they have no known competing financial interests or personal relationships that could have appeared to influence the work reported in this paper.

Acknowledgment

This work was supported by 2024 (RFO) Ricerca Fondamentale Orientata – University of Bologna, Italy. The authors wish to thank Dr. Luciano Callipo of Agilent Technologies for his technical support.

Appendix A. Supplementary data

Supplementary data to this article can be found online at https://doi.org/10.1016/j.talanta.2025.129346.

Data availability

Data will be made available on request.

References

[1] E. Carrilho, A.W. Martinez, G.M. Whitesides, Understanding wax printing: a simple micropatterning process for paper-based microfluidics, Anal. Chem. 81 (2009) 7091–7095, https://doi.org/10.1021/ac901071p.

[2] E. Noviana, T. Ozer, C.S. Carrell, J.S. Link, C. McMahon, I. Jang, C.S. Henry, Microfluidic paper-based analytical devices: from design to applications, Chem. Rev. 121 (2021) 11835–11885, https://doi.org/10.1021/acs.chemrev.0c01335.

[3] P. Lingadharini, D. Maji, Eco-sustainable point-of-care devices: progress in paper and fabric based electrochemical and colorimetric biosensors, Talanta 285 (2024) 127397, https://doi.org/10.1016/j.talanta.2024.127397.

[4] B. Selvakumar, A. Kathiravan, Sensory materials for microfluidic paper based analytical devices – a review, Talanta 235 (2021) 122733, https://doi.org/10.1016/j.talanta.2021.122733.

[5] Z. Yao, P. Coatsworth, X. Shi, J. Zhi, L. Hu, R. Yan, H.D. Yu, Paper-based sensors for diagnostics, human activity monitoring, food safety and environmental detection, Sens. Diagn 1 (2022) 312–342, https://doi.org/10.1039/D2SD00017B.

[6] Y. Lu, W. Shi, L. Jiang, J. Qin, B. Lin, Rapid prototyping of paper-based microfluidics with wax for low-cost, portable bioassay, Electrophoresis 30 (2009) 1497–1500, https://doi.org/10.1002/elps.200800563.

[7] S. Malik, J. Singh, K. Saini, V. Chaudhary, A. Umar, A.A. Ibrahim, S. Baskoutas, Paper-based sensors: affordable, versatile, and emerging analyte detection platforms, Anal. Methods 16 (2024) 2777–2809, https://doi.org/10.1039/D3AY02258G.

[8] N. Gautam, R. Verma, R. Ram, J. Singh, A. Sarkar, Development of a biodegradable microfluidic paper-based device for blood-plasma separation integrated with non-enzymatic electrochemical detection of ascorbic acid, Talanta 266 (2024) 125019, https://doi.org/10.1016/j.talanta.2023.125019.

[9] S. Wang, W.J. Chen, A. Du, Y. Kou, X. Xu, D. Hu, Z. Lu, Advances in paper-based analytical devices relying on optical detection, Adv. Compos. Hybrid Mater. 8 (2025) 260, https://doi.org/10.1007/s42114-025-01333-x.

[10] A. Isa, M. Gharibi, A. Cetinkaya, S.A. Ozkan, Sustainable and scalable detection: paper-based analytical devices and miniaturized detection systems for modern diagnostics, Microchem. J. 201 (2025) 113210, https://doi.org/10.1016/j.microc.2025.113210.

[11] Y. Jiang, Z. Hao, Q. He, H. Chen, A simple method for fabrication of microfluidic paper-based analytical devices and on-device fluid control with a portable corona generator, RSC Adv. 6 (2016) 2888–2894, https://doi.org/10.1039/C5RA23470K.

[12] L. Bezinge, C.J. Shih, D.A. Richards, A.J. Demello, Electrochemical paper-based microfluidics: harnessing capillary flow for advanced diagnostics, Small 20 (2024) 2401148, https://doi.org/10.1002/smll.202401148.

[13] F. Arduini, Paper as a sustainable material for smart electrochemical (bio)sensors with unprecedented features: a perspective, Anal. Chem. 97 (2025) 10126–10138, https://doi.org/10.1021/acs.analchem.5c00128.

[14] E.L. Fava, T.A. Silva, T.M. do Prado, F.C. de Moraes, R.C. Faria, O. Fatibello-Filho, Electrochemical paper-based microfluidic device for high throughput multiplexed analysis, Talanta 203 (2019) 280–286, https://doi.org/10.1016/j.talanta.2019.05.081.

[15] Y. Yang, E. Noviana, M.P. Nguyen, B.J. Geiss, D.S. Dandy, C.S. Henry, Paper-Based microfluidic devices: emerging themes and applications, Anal. Chem. 89 (2017) 71–91, https://doi.org/10.1021/acs.analchem.6b04581.

[16] A. Luongo, A.R. von Stockert, F.D. Scherag, T. Brandstetter, M. Biesalski, J. Rühe, Controlling fluorescent readout in paper-based analytical devices, ACS Biomater. Sci. Eng. 9 (2023) 6379–6389, https://doi.org/10.1021/acsbiomaterials.3c00736.

[17] G.G. Morbioli, T. Mazzu-Nascimento, A.M. Stockton, E. Carrilho, Technical aspects and challenges of colorimetric detection with microfluidic paper-based analytical devices (μPADs) – a review, Anal. Chim. Acta 970 (2017) 1–22, https://doi.org/10.1016/j.aca.2017.03.037.

[18] S. Kanchi, M.I. Sabela, P.S. Mdluli, K. Bisetty, Smartphone based bioanalytical and diagnosis applications: a review, Biosens. Bioelectron. 102 (2018) 136–149, https://doi.org/10.1016/j.bios.2017.11.021.

[19] N. Uhlikova, M.I.G. Almeida, I. McKelvie, R. Morrison, S.D. Kolev, Use of scanners for colorimetric analysis of microfluidic paper-based analytical devices (μPADs): a practical guide, Microchem. J. 191 (2023) 108879, https://doi.org/10.1016/j.microc.2023.108879.

[20] R. Catalan-Carrio, T. Akyazi, L. Basabe-Desmonts, F. Benito-Lopez, Predicting dimensions in microfluidic paper-based analytical devices, Sensors 21 (2020) 101, https://doi.org/10.3390/s21010101.

[21] I. Macleod Briongos, Z.D. Call, C.S. Henry, D.L. Bark Jr., Maximizing flow rate in single paper layer, rapid flow microfluidic paper-based analytical devices, Microfluid. Nanofluidics 27 (2023) 70, https://doi.org/10.1007/s10404-023-02679-8.

[22] M. Ali, A.T. Jafry, H. Abbas, H. Ullah, Flow control in paper-based microfluidic channel by using hydrophobic tape barrier on the paper surface, MATEC Web Conf. 381 (2023) 01009, https://doi.org/10.1051/matecconf/202338101009.

[23] K. Lv, Y. Zhang, K. Tang, W. Huang, F. Chen, M. Chen, J. Zhang, A machine learning-driven cyclic optimizing strategy for the construction of paper-based microfluidic devices in the early diagnosis of periodontitis, ACS Sens. (2025), https://doi.org/10.1021/acssensors.5c02031.

[24] G.A. Lewis, D. Mathieu, R. Phan-Tan-Luu, Pharmaceutical Experimental Design, CRC Press, Boca Raton, FL, USA, 2019, https://doi.org/10.1201/9780203508688.

[25] ICH guideline Q14 - analytical procedure development. https://database.ich.org/sites/default/files/ICH_Q14_Guideline_2023_1116_1.pdf, 2022. (Accessed 13 October 2025).

[26] Y. Beguin, A. Jaspers, Iron sucrose – characteristics, efficacy and regulatory aspects of an established treatment of iron deficiency and iron-deficiency anemia in a broad range of therapeutic areas, Expet Opin. Pharmacother. 15 (2014) 2087–2103, https://doi.org/10.1517/14656566.2014.953928.

[27] U.S. Pharmacopeia, National formulary USP 38—NF 33, in: Rockville: the United States Pharmacopeial Convention, 2015.

[28] J.I. Aguiar, S.O. Ribeiro, A. Leite, M. Rangel, A.O. Rangel, R.B. Mesquita, Iron determination in natural waters using a synthesised 3-hydroxy-4-pyridione ligand in a newly developed microfluidic paper-based device, Chemosensors 11 (2023) 101, https://doi.org/10.3390/chemosensors11020101.

[29] S. Dortez, A.G. Crevillen, A. Escarpa, Integrated calibration and serum iron in situ analysis into an array microfluidic paper-based analytical device with smartphone readout, Talanta 253 (2023) 123914, https://doi.org/10.1016/j.talanta.2022.123914.

[30] F.T. Ferreira, K.A. Catalão, R.B. Mesquita, A.O. Rangel, New microfluidic paper-based analytical device for iron determination in urine samples, Anal. Bioanal. Chem. 413 (2021) 7463–7472, https://doi.org/10.1007/s00216-021-03706-9.

[31] R.B. Mesquita, C. Klima, H. Martínez-Pérez-Cejuela, A.R. Monforte, A.S. Ferreira, A.O. Rangel, Targeting iron speciation in wines: design of a microfluidic paper-based device for determination of iron (II) and iron (III), Microchem. J. 188 (2023) 108462, https://doi.org/10.1016/j.microc.2023.108462.

[32] K. Shrivas, Monisha, T. Kant, I. Karbhal, R. Kurrey, B. Sahu, D. Sinha, G.K. Patra, M.K. Deb, S. Pervez, Smartphone coupled with paper-based chemical sensor for on-site determination of iron (III) in environmental and biological samples, Anal. Bioanal. Chem. 412 (2020) 1573–1583, https://doi.org/10.1007/s00216-019-02385-x.

[33] R. Gotti, J. Fiori, L. Liverani, F. Spelta, Capillary electrophoresis method for speciation of iron (II) and iron (III) in pharmaceuticals by dual precapillary complexation, Electrophoresis 36 (2015) 2820–2827, https://doi.org/10.1002/elps.201500235.

[34] S. Fütterer, I. Andrusenko, U. Kolb, W. Hofmeister, P. Langguth, Structural characterization of iron oxide/hydroxide nanoparticles in nine different parenteral drugs for the treatment of iron deficiency anaemia by electron diffraction (ED) and X-ray powder diffraction (XRPD), J. Pharm. Biomed. Anal. 86 (2013) 151–160, https://doi.org/10.1016/j.jpba.2013.08.005.

[35] G.L. Smith, A.A. Reutovich, A.K. Srivastava, R.E. Reichard, C.H. Welsh, A. Melman, F. Bou-Abdallah, Complexation of ferrous ions by ferrozine, 2, 2′-bipyridine and 1, 10-phenanthroline: implication for the quantification of iron in biological systems, J. Inorg. Biochem. 220 (2021) 111460, https://doi.org/10.1016/j.jinorgbio.2021.111460.

[36] H. Najarzadekan, H. Sereshti, Transparent polycaprolactam electrospun nanofibers doped with 1, 10-phenanthroline optical sensor for colorimetric determination of iron (II) and vitamin C, Fibers Polym. 19 (2018) 2149–2156, https://doi.org/10.1007/s12221-018-7568-6.

[37] P.F.F. Lovato, E.S. Chaves, L.N. Vidal, P.M. Santos, Feasibility of digital image colorimetric methods for iron determination in river sediment, Int. J. Sediment Res. 39 (2024) 714–719, https://doi.org/10.1016/j.ijsrc.2024.02.005.

[38] G. Wendimu, A. Hussen, Wax screen-based fabrication of paper devices for the determination of iron in particulates of selected welding fumes in Addis Ababa, Ethiopia, Bull. Chem. Soc. Ethiop. 38 (2024) 563–576, https://doi.org/10.4314/bcse.v38i3.2.

[39] G. Musile, C. Grazioli, S. Fornasaro, N. Dossi, E.F. De Palo, F. Tagliaro, F. Bortolotti, Application of paper-based microfluidic analytical devices (μPAD) in forensic and clinical toxicology: a review, Biosensors 13 (2023) 743, https://doi.org/10.3390/bios13070743.

[40] ICH Guideline Q9(R1) - quality risk management. https://database.ich.org/sites/default/files/ICH_Q9%28R1%29_Guideline_Step4_2025_0115.pdf, 2005. (Accessed 13 October 2025).

[41] ICH Guideline Q2(R2), Validation of Analytical Procedures, 2022. https://database.ich.org/sites/default/files/ICH_Q2%R2_Document_Step2_Guideline_2022_0324.pdf. (Accessed 13 October 2025).

[42] P. Aryal, E. Brack, T. Alexander, C.S. Henry, Capillary flow-driven microfluidics combined with a paper device for fast user-friendly detection of heavy metals in water, Anal. Chem. 95 (2023) 5820–5827, https://doi.org/10.1021/acs.analchem.3c00378.

[43] K. Ogawa, T. Kaneta, Determination of iron ion in the water of a natural hot spring using microfluidic paper-based analytical devices, Anal. Sci. 32 (2016) 31–34, https://doi.org/10.2116/analsci.32.31.

[44] H. Asano, Y. Shiraishi, Development of paper-based microfluidic analytical device for iron assay using photomask printed with 3D printer for fabrication of hydrophilic and hydrophobic zones on paper by photolithography, Anal. Chim. Acta 883 (2015) 55–60, https://doi.org/10.1016/j.aca.2015.04.014.

[45] D. Merli, A. Profumo, C. Dossi, An analytical method for Fe(II) and Fe(III) determination in pharmaceutical grade iron sucrose complex and sodium ferric gluconate complex, J. Pharm. Anal. 2 (2012) 450–453, https://doi.org/10.1016/j.jpha.2012.05.003.